HHS Public Access

Author manuscript

Hepatology. Author manuscript; available in PMC 2017 November 01.

Published in final edited form as:

Hepatology. 2016 November ; 64(5): 1518–1533. doi:10.1002/hep.28676.

Receptor Interacting Protein 3 Protects Mice from High Fat Diet-Induced Liver Injury

Sanjoy Roychowdhury[1,5], **Rebecca L. McCullough**[1], **Carlos Sanz-Garcia**[1], **Paramananda Saikia**[1], **Naim Alkhouri**[2,3], **Ammar Matloob**[3], **Katherine Pollard**[1], **Megan R. McMullen**[1], **Colleen M. Croniger**[4], and **Laura E. Nagy**[1,2,4,5]

[1]Center for Liver Disease Research, Department of Pathobiology, Cleveland Clinic, Cleveland, Ohio

[2]Department of Gastroenterology, Cleveland Clinic, Cleveland, Ohio

[3]Department of Pediatric Gastroenterology, Cleveland Clinic, Cleveland, Ohio

[4]Department of Nutrition, Case Western Reserve University, Cleveland, Ohio

[5]Department of Molecular Medicine, Case Western Reserve University, Cleveland, Ohio

Abstract

Multiple pathways of programmed cell death are important in liver homeostasis. Hepatocyte death is associated with progression of nonalcoholic fatty liver disease (NAFLD) and inhibition of apoptosis partially protects against liver injury in response to high fat diets (HFD). However, the contribution of necroptosis, a caspase-independent pathway of cell death, to HFD-induced liver injury is not known. Wild-type C57BL/6 and receptor interacting protein (RIP) 3−/− mice were randomized to chow or HFD. HFD-fed C57BL/6 mice increased expression of RIP3, the master regulator of necroptosis, as well as phosphorylated mixed lineage kinase domain-like (pMLKL), an effector of necroptotic cell death, in liver. HFD did not increase pMLKL in RIP3−/− mice. HFD increased fasting insulin and glucose, as well as glucose intolerance, in C57BL/6 mice. RIP3−/− were glucose intolerant even on chow diets; HFD further increased fasting glucose and insulin, but not glucose intolerance. HFD also increased hepatic steatosis, plasma ALT activity, inflammation, oxidative stress and hepatocellular apoptosis in wild-type mice; these responses were exacerbated in RIP3−/− mice. Importantly, increased inflammation and injury was associated with early indicators of fibrosis in RIP3−/− compared to C57BL/6 mice. Culture of AML12 hepatocytes with palmitic acid increased cytotoxicity via apoptosis and necrosis. Inhibition of RIP1 with necrostatin-1 or siRNA knock-down of RIP3 reduced palmitic acid-induced cytotoxicity.

Conclusion—Absence of RIP3, a key mediator of necroptosis, exacerbated HFD-induced liver injury, associated with increased inflammation and hepatocyte apoptosis, as well as early fibrotic responses. These findings indicate that shifts in the mode of hepatocellular death can influence disease progression and have therapeutic implications because manipulation of hepatocyte cell death pathways is being considered as a target for treatment of NAFLD.

Corresponding Author: Laura E. Nagy, PhD, Department of Pathobiology and Gastroenterology, Cleveland Clinic/ LRI NE40, 9500 Euclid Avenue, Cleveland, Ohio 44195, nagyL3@ccf.org.

Keywords

Necroptosis; high-fat diet; liver injury; apoptosis

Apoptosis is a highly controlled biological process that has generally been considered non-inflammatory because of the rapid removal of apoptotic cells by phagocytic cells (1). However, accumulating evidence suggests that, within the context of liver disease, hepatocyte apoptosis may trigger a response of cell repair, inflammation, regeneration, and fibrosis (2). Engulfment of apoptotic bodies from dying hepatocytes by hepatic stellate cells (HSC) stimulates their fibrogenic activity (3) and increasing hepatocyte apoptosis by hepatocyte-specific deletion of anti-apoptotic genes leads to fibrosis (4, 5). Indeed, an increase in hepatocyte apoptosis has emerged as a central mechanism involved in the development of nonalcoholic fatty liver disease (NAFLD) and its progression from nonalcoholic fatty liver (NAFL) to nonalcoholic steatohepatitis (NASH) (6). Interestingly, the inhibition of hepatocyte apoptosis only partially protects against high fat diet (HFD)-induced liver steatosis and injury (7) suggesting that alternative modes of cell death might also be important in the progression of NAFLD.

Necroptosis is a newly described form of programmed cell death that uses many of the same upstream activation pathways as apoptosis but morphologically resembles necrosis (8, 9). Necroptosis may serve as a backup pathway to enable cell death when apoptosis is inhibited (10) and the decision whether a cell undergoes apoptosis or necroptosis is dependent on the interaction between receptor interacting protein kinases (RIP) 1/ RIP3 and caspase-8 (2). Necroptosis is an alternative programmed cell death pathway that may have evolved to control infections by viruses that express caspase-inhibitors, thus preventing apoptosis of infected cells (11). Necroptosis results in cell swelling and rupture, releasing potentially pro-inflammatory cellular contents (11). While apoptosis requires the activation of caspases, necroptosis is driven by the activity of RIP1 and RIP3 kinases, resulting in the phosphorylation of mixed lineage kinase domain-like (MLKL). Necroptosis is activated by innate immune signals, including TNFα, toll-like receptor (TLR) 3 and TLR4 ligands, as well as DNA-dependent activator of interferon regulatory factors (DAI) (12). Interestingly, many of the same effector proteins are involved in programmed cell death via apoptosis and necroptosis (12). It is the functional regulation of these common players that drives a cell to form the apoptosome, leading to activation of apoptosis. or to formation of the necrosome, to drive necroptotic cell death (13).

Recent evidence suggests that RIP3-dependent necroptosis is activated in multiple types of liver injury, including early acetaminophen hepatotoxicity (14) and chronic ethanol-induced liver injury (15), as well as ischemia-reperfusion injury, inflammatory bowel disease and atherosclerosis (12). While RIP3 is not highly expressed by hepatocytes in healthy liver, its expression is increased in patients with alcoholic liver disease (15), hepatitis B and C patients (16), as well as NASH patients, but not those with simple steatosis (16, 17). In murine models of liver injury, RIP3-deficiency protects mice from both acetaminophen and ethanol-induced liver injury (14, 15). Similarly, RIP3 is reported to contribute to liver injury and disease progression in the methionine- and choline-deficient (MCD) diet-induced model

of NASH (16, 17). However, the contribution of RIP3 in high-fat diet-induced models of NAFLD has not yet been studied.

There are important differences in the pathophysiology of liver injury between high-fat diet- and MCD diet-induced liver injury. The MCD diet results in liver injury that is morphologically similar to human NASH; however, it does not induce the systemic glucose intolerance and insulin resistance characteristic of patients with NAFLD. Further, mice tend to lose weight on the MCD diet rather than gain weight, as is typical of obesity-driven NAFLD (18). In contrast, mice on high-fat diets become obese, exhibit glucose intolerance and indications of insulin resistance and may therefore represent a more appropriate model for study of the mechanisms for the development of NAFLD (18).

Given the central role of programmed cell death in the pathogenesis of NAFLD and its progression to hepatic fibrosis, the objective of the current investigation was to assess the role of RIP3-dependent necroptosis in the pathophysiology of high-fat diet (HFD)-induced liver injury using a genetically-deficient mouse model. In contrast to the injurious contributions of RIP3 to liver injury in response to the MCD diet, our studies reveal that RIP3 actually protects mice from HFD-induced liver injury.

Materials and Methods

Additional methods and Materials are included as Supplemental Material

Animals and care

Five week old male wild-type mice (C57BL/6) were purchased from Jackson Laboratory (Bar Harbor, ME). RIP3−/− mice were a generous gift from Vishva Dixit (Genentech, San Fransisco, CA) (19). Studies were done both in the originally generated RIP3−/− strain, as well as in a more recently derived RIP3−/− strain in which the neomycin cassette used for cloning was deleted. Both strains are on a C57BL/6 background.

All animals received humane care and all procedures were approved by the Cleveland Clinic Institutional Animal Care and Use Committee. C57BL/6 and RIP3−/− mice were fed a high-fat diet (HFD) containing 42% kcal from fat, 18.8 kJ/g (TD 88137 Teklad Mills, Madison, WI) or a standard control diet (Chow) containing 6% fat, 13.0 kJ/g (TD 2918, Teklad Mills, Madison, WI).

Histopathology and immunohistochemistry of mouse liver and adipose

Formalin-fixed tissues were paraffin-embedded, sectioned, coded and stained with H&E. Apoptosis was detected using a terminal deoxynucleotidyl transferase dUTP nick end labeling (TUNEL) assay as described previously (20). Formalin-fixed paraffin-embedded liver sections were de-paraffinized and stained for caspase-generated fragments of cytokeratin-18 (M30), RIP3, pMLKL, collagen 1α, α-SMA, 4-hydroxynonenal, TNFα or F4/80 (21). For histological detection of fibrosis, liver tissues were stained with Sirius Red. Frozen liver sections were stained with oil red O. All images presented in the results are representative of at least 3 images per liver and 4–6 mice per experimental condition. Images

were analyzed and semi-quantified using Image Pro Plus software (Media Cybernetics, Bethesda, MD).

Statistical Analysis

Values were reported as means ± SEM and each group included 4–6 mice, except for Figure 4A where two feeding trials were combined for an n=9–12.. Data were analyzed by analysis of variance (ANOVA) using the general linear models procedure and follow-up comparisons were made by least square means testing. (SAS, Carey, IN). Normality was assessed by the Shapiro-Wilks test and data were log-transformed when necessary to obtain a normal distribution. Non-parametric ANOVA tests were used for data sets that were not normally distributed (Graph Pad Prism). For all data, differences were considered statistically significant at a $p< 0.05$. Unless indicated otherwise in the figure legends, values with different alphabetical superscripts were significantly different from each other, $p< 0.05$.

Results

High-fat diet increases the expression of RIP3 and phosphorylation of MLKL in mouse liver

To evaluate the role of RIP3 in HFD-induced NAFLD, RIP3 expression in liver was visualized by immunohistochemistry in chow-fed and HFD-fed wild-type mice (Figure 1A/C). RIP3−/− mice were included as negative controls (Figure 1B). HFD feeding to C57BL/6 mice increased the expression of RIP3 in liver tissue (Figure 1A/C); immunoreactivity was primarily associated with lipid-laden hepatocytes (Figure 1A insets). MLKL is a down-stream target of RIP3 and is an important effector in necroptotic cell death. HFD feeding to wild-type mice increased phospho-MLKL quantity by Western blot (Figure 1D) and immunohistochemistry (Figure 1E). MLKL−/− mice did not exhibit pMLKL immunoreactivity (Figure 1E). This increase in expression is consistent with increased RIP3 (16,17) and pMLKL immunoreactivity in liver biopsies from NASH patients (22).

RIP3-Deficiency Exacerbated HFD-Induced Hepatocellular Injury and Steatosis

If expression of RIP3 was critical to the development of HFD-induced liver injury, then RIP3-deficient mice should be protected from injury. We investigated the effects of HFD feeding for 6 or 12 weeks in C57BL/6 and RIP3−/− mice. Two different strains of RIP3−/− were used. The first is the original RIP3−/− developed by Dixit and colleagues (19); this strain still retains the neomycin cassette used for cloning and is the strain used by many groups in previous studies (termed here RIP3−/− (neo)). The second strain is a newly developed line by Dixit and colleagues in which the neomycin cassette has been deleted (termed here RIP3−/− (CREΔ)).

Both male (Figure 2A/B and 2C/D) and female (Figure2E/F) C57BL/6 mice exhibited increased ALT/AST concentrations in the plasma (Figure 2A/C/E), as well as increased concentrations of hepatic triglycerides after HFD (Figure 2B/D/F). Males from both RIP3−/− (neo) and RIP3−/− (CREΔ) strains also had increased ALT/AST concentrations and hepatic triglycerides compared to C57BL/6 mice (Figure 2 A–D). This exacerbation of

ALT/AST was observed in RIP3−/− (neo) mice as early as 6 weeks of HFD feeding (Figure 2A). Pathological scoring of steatosis in hepatocytes (Supplemental Figure 1A), as well as Oil Red O staining (Supplemental Figure 1B) were also increased to a greater extent in RIP3−/− (neo) compared to C57BL/6 in response to HFD feeding for 12 weeks. Since both strains of RIP3−/− mice responded similarly to the HFD feeding protocol, we focused our studies on the RIP3−/− (neo) strain, as this line has been the most well studied line in previous literature. In all subsequent figures, RIP3−/− refers to the RIP3−/ (neo) strain.

Metabolic profiles of C57BL/6 and RIP3−/− mice fed High-Fat Diets

Food intake in males did not differ between genotypes and both C57BL/6 and RIP3−/− male mice gained more weight on HFD compared to chow diets (Supplemental Figure 2A/B). However, RIP3−/− (neo) and RIP3−/− (CREΔ) both gained more weight than C57BL/6 on the HFD (Supplemental Figure 2A/B). Energy expenditure and activity levels were assessed in C57BL/6 and RIP3−/− (neo) in metabolic chambers. There was no difference in activity levels between genotypes on either the chow or HFD (data not shown) and energy expenditure was not different between genotypes on either the chow or HFD (Supplemental Figure 2C).

Fasting glucose concentrations were higher in RIP3−/− mice on chow diets and both RIP3−/− and C57BL/6 mice had a similar increase in fasting glucose concentrations in response to 12 wks of HFD feeding (Figure 3A). Fasting insulin and HOMA-IR were increased with HFD feeding to wild-type mice; RIP3−/− already had elevated fasting insulin and HOMA-IR at baseline; these parameters were further increased by almost 5-fold in response to HFD feeding (Figure 3A). Fasting glucose tolerance tests were carried out after 14 weeks of HFD feeding. Consistent with their elevated fasting glucose and insulin concentrations on the chow diet, RIP3−/− mice were more glucose intolerant than C57BL/6 mice on chow diets (Figure 3B/C). However, while C57BL/6 mice became glucose intolerant in response to HFD, the area under the glucose tolerance curves did not deteriorate further in response to HFD in the RIP3−/− mice (Figure 3B/C). Plasma indicators of lipid metabolism were assessed (Figure 3D). Circulating TG were decreased in RIP3−/− mice after HFD and NEFA were not increased in response to HFD; both these responses are consistent with an increased TG storage in the liver in RIP3−/− compared to wild-type mice (Figure 3D).

Indicators of insulin signaling, glucose homeostasis and fatty acid metabolism in RIP3−/− mice compared to wild-type mice

Since the liver is an important contributor to glucose homeostasis, we investigated insulin signaling responses in the liver. Serine phosphorylation of IRS-1 is associated with impaired insulin receptor tyrosine kinase signaling. Total IRS-1 protein was decreased and serine^{307}-phosphorylation of IRS-1 relative to total IRS-1 was higher in RIP3−/− mice after HFD compared to chow-fed RIP3−/− and wild-type mice (Figure 4A). In order to better characterize the spectrum of changes in gene expression between wild-type and RIP3−/− livers in response to HFD, we carried out an array analysis of expression of mRNA involved in glucose and fatty acid metabolism in livers of chow and HFD fed wild-type and RIP3−/− mice (Figure 4B). Of the genes investigated related to glucose homeostasis, 13 genes were up-regulated by more than 2-fold in RIP3−/− mice compared to wild-type mice. After HFD

feeding, there was a further exacerbation of gene expression related to glucose and fatty acid metabolism, with 26 genes increased by more than 2-fold. We confirmed a number of these changes in gene expression by qPCR (Figure 4C).

Indicators of liver and adipose tissue inflammation were elevated in RIP3−/− mice

An increased inflammatory milieu in liver and adipose tissue are hallmarks of HFD-induced NAFLD. PCR array analysis revealed that expression of multiple genes associated with inflammation were increased in chow-fed RIP3−/− mice compared to wild-type and that inflammatory gene expression was again exacerbated in response to HFD feeding (Figure 5A/Supplemental Table 1). These results were confirmed by qPCR (Figure 5A). RIP3-deficiency enhanced HFD-induced increases in expression of TNFα, IL-1β and MCP-1, but not IL-6 or F4/80, mRNA. Expression of TNFα, assessed by immunohistochemistry, tended to be increased in RIP3−/− mice even on chow diets and was significantly elevated in response to HFD (Figure 5B). Expression of immunoreactive TNFα was predominantly localized to areas of heavily lipid-laden hepatocytes (Figure 5B). HFD diet feeding also resulted in a greater accumulation of 4-hydroxynonenal adducts, an indicator of oxidative stress, in HFD-fed RIP3−/− compared to wild-type mice (Figure 5C). In adipose tissue, RIP3-deficiency similarly exacerbated HFD-induced increases in expression of TNFα and MCP-1, but not IL-6, mRNA (Figure 5D). In contrast to the liver, expression of F4/80 mRNA (Figure 5D) and protein (Figure 5E) were increased in C57BL/6 mice after HFD feeding and further increased in RIP3−/− mice. The presence of crown structures was also apparent in both C57BL/6 and RIP3−/− mice, but at a higher density in RIP3−/− mice compared to wild-type (Figure 5F).

RIP3-deficiency decreased phosphorylation of MLKL, but was associated with increased hepatocellular apoptosis

Phosphorylation of MLKL is a critical event down-stream of RIP3 in the necroptotic pathway and phospho-MLKL has been suggested as a useful biomarker of necroptosis (22). HFD feeding to wild-type mice increased phospho-MLKL immunoreactivity in the liver; this response was abrogated in RIP3−/− mice (Figure 6A). Given the close interplay between apoptosis and necroptosis in many cell types, we next evaluated whether the absence of RIP3 influenced the interaction between HFD and apoptosis in liver. HFD feeding increased TUNEL staining in wild-type mice; this response was further exacerbated in RIP3−/− mice (Figure 6B). TUNEL staining was co-localized with F4/80, a marker of resident macrophages in the liver, in some cells (Supplemental Figure 3); however, the majority of TUNEL positive cells did not co-localize with F4/80 in either wild-type or RIP3−/− mice. Accumulation of M30, a cleavage product of CK18, is a specific marker of hepatocyte caspase activation and apoptosis; M30 accumulation was increased by HFD feeding in both genotypes, but the response was exacerbated in RIP3−/− mice (Figure 6C).

Palmitic acid-induced lipotoxicity occurred via multiple cell death pathways in hepatocytes

In order to better understand the mechanistic contributions of RIP3 to hepatocyte cell death, AML12 hepatocytes were cultured with palmitic acid to dose-dependently increase cytotoxicity (Figure 7A). Palmitic acid-induced lipotoxicity is mediated, at least in part, via lysosomal pathways leading to caspase activation (2). Inhibition of caspases (with Z-VAD),

RIP1 (with necrostatin-1) or cathepsin B (CA-074) each reduced palmitic acid-induced cytotoxicity (Figure 7B); combinations of inhibitors lead to additive effects in suppressing lipotoxicity (Figure 7B). Pre-treatment with Z-VAD, but not necrostatin-1, prevented palmitic acid-induced caspase-3 and poly ADP ribose polymerase (PARP) cleavage (Figure 7C). PARP cleavage was also reduced by CA-074, while caspase-3 cleavage after CA-074 pre-treatment was intermediate, not different from either basal or palmitic acid-treated cells (Figure 7C). siRNA knock-down of RIP3 suppressed RIP3 protein expression (Supplemental Figure 4) and reduced palmitic acid-induced cytotoxicity (Figure 7D) to a similar extent as pre-treatment with necrostatin-1 (Figure 7B); siRNA knock-down of RIP3 also decreased propidium iodine staining (Figure 7F), but not caspase-3 cleavage (Figure 7E). Taken together, these data indicate that palmitic acid-induced cytotoxicity in AML12 cells occurs via both caspase-dependent and independent pathways; necrostatin-1 or siRNA knock-down of RIP3 protects cells from caspase-independent cytotoxicity.

RIP3-deficient mice exhibit increased early fibrosis compared to C57BL/6 after high fat diet feeding

Inflammation and hepatocyte apoptosis are critical drivers of fibrosis in liver, due, at least in part, to the activation of hepatic stellate cells in response to phagocytosis of apoptotic hepatocytes (6). Importantly, increased inflammation and hepatocyte apoptosis in RIP3−/− mice were associated with increased liver fibrosis. Sirius red staining of extracellular matrix was modestly increased in response to HFD feeding in wild-type mice, but increased more extensively in RIP3−/− mice (Figure 8A/B and Supplemental Figure 5A). Collagen 1 accumulation was also increased to a greater degree in RIP3−/− in response to HFD compared to wild-type mice (Supplemental Figure 5B). Similarly, accumulation of α-smooth muscle actin (αSMA) was mildly increased in wild-type, but more robustly increased in RIP3−/− mice in response to HFD feeding (Figure 8C/D). Consistent with these indicators of fibrosis, expression of mRNA for collagen-1α1, αSMA and matrix metalloproteinase 13 (MMP13), but not MMP9, were increased to a greater extent in RIP3−/− compared to C57BL/6 in response to HFD (Figure 8E).

Discussion

NAFLD is the hepatic manifestation of obesity and insulin resistance; progression involves the development of liver steatosis, increased inflammation and hepatocyte injury, and eventually the deposition of extracellular matrix proteins leading to liver fibrosis and cirrhosis. The direct association between programmed cell death and progression of NAFLD is well established; however, the distinct contribution of different programmed cell death pathways to liver injury and fibrosis is not completely understood. In the current study, HFD feeding increased the expression of RIP3, as well as the phosphorylation of MLKL, in mouse liver, suggesting a role for necroptosis in the pathogenesis of NAFLD. However, genetic deletion of RIP3 increased hepatic steatosis and ALT/AST, inflammation and apoptosis in liver, as well as hepatic fibrosis in response to HFD. Taken together, these data suggest that inhibition of necroptosis shifts the equilibrium of programmed cell death to increased apoptosis, which in turn, exacerbates the fibrotic response to HFD feeding.

Cell death pathways of apoptosis and necroptosis utilize some of the same effector molecules; apoptosis and necroptosis may function as “reciprocal back-up” pathways of cell death. For example, in some types of cultured cells, inhibition of necroptosis with necrostatin-1 shifts cell death from necroptosis to apoptosis (23). Similarly, inhibition of apoptosis due to low caspase-8 activity shifts cells to necroptosis (24). The mechanisms for this switch are not understood, but are under active investigation in a number of laboratories. Kaiser’s group recently proposed that RIP3 regulates the balance between apoptosis and necroptosis via the recruitment of various effectors to its RHIM domain (25). Interestingly, while RIP3−/− mice exhibited lower phosphorylation of MLKL, consistent with decreased necroptosis, apoptosis in RIP3−/− livers was increased in response to HFD when compared to wild-type mice. A shift towards more apoptosis in the absence of RIP3 could potentially occur via two mechanisms: a mechanism intrinsic to changes in hepatocyte metabolism in the absence of RIP3 or as a consequence of increased inflammatory/oxidative injury. If a hepatocyte intrinsic pathway were involved, then we would expect that palmitic acid-induced apoptosis would be increased in cultured hepatocytes lacking RIP3 or treated with necrostatin-1, to inhibit RIP1 and prevent necroptosis. However, treatment with necrostatin-1 or siRNA knock-down of RIP3 prevented cytotoxicity/propidium iodine uptake without affecting caspase-3 cleavage. Taken together, these data suggest that increased apoptosis *in vivo* in RIP3−/− mice after HFD feeding is not an intrinsic response of hepatocytes, but instead requires additional *in vivo* signals. It is likely that the increased inflammatory milieu, combined with increased oxidative stress, within the liver of the RIP3−/− mice leads to more apoptosis compared to wild-type mice.

RIP3 has been associated with a number of different functions. For example, RIP3 can interact with mitochondrial energy metabolism, generating excess ROS, which in turn can contribute to necroptosis (9). However, in the context of HFD, accumulation of 4-HNE, an indicator of oxidative stress, was exacerbated by deficiency of RIP3. These data suggest that the contribution of RIP3 to the direct generation of excess ROS is likely masked by more dominant drivers of oxidative stress, such as inflammatory responses, generated in response to HFD. Similarly, RIP3 can drive the activation of inflammasomes (24); however, in response to HFD, absence of RIP3 increased expression of IL1β, suggesting that RIP3 is not the primary driver of inflammasome activation in the context of HFD feeding.

Apoptosis is considered a driving force of NAFLD-induced liver fibrosis; apoptotic hepatocytes are phagocytosed by HSC, leading to their activation to a collagen-producing myofibroblast phenotype. Recent work has pioneered the use of serum biomarkers for hepatocyte apoptosis, such as cytokeratin-18 and soluble Fas, to diagnose more advanced stages NAFLD in both adults and children (26). Inhibiting apoptosis through a pan-caspase inhibitor VX-166 reduced the progression of liver fibrosis in the MCD diet model for NASH in mice (27). Importantly, inhibition of caspase activity did not improve liver injury as assessed by ALT, suggesting that caspase-independent pathways of hepatocellular injury are important contributors to NASH progression (27). More recent studies, also utilizing the MCD model of NASH, identified RIP3-mediated necroptosis as a critical contributor to MCD-induced liver injury (16, 17). These results contrast with the protective function of RIP3 identified in our study making use of HFD-induced model of NAFLD. It is important to note that differences in the source of CD57/BL6 wild-type mice used in these different

studies may limit comparisons between models; Afonso, et al (16) used C57BL/6 mice purchased from Taconic, Gautheron, et al., (17) used littermates from caspase-8 floxed mice and we purchased C57BL/6 mice from Jackson.

While the MCD model of NASH morphologically resembles human NASH, the pathophysiology to injury is quite distinct. In order to understand the interplay between caspase-dependent and RIP3-dependent pathways of cell death in the context of the obese metabolic phenotype, we conducted our studies in mice fed a HFD. Mice on the HFD gained more weight than chow-fed, were glucose intolerant and exhibited indications of impaired hepatic glucose homeostasis. Importantly, our data indicate that, within the context of HFD-induced obesity, RIP3 serves an anti-inflammatory, anti-apoptotic and anti-fibrotic function. These data are consistent with the concept that specific cellular death pathways are highly dependent on state of cellular metabolism (28). Indeed, recent data suggest that activation of a specific death receptor may initiate either apoptosis or necroptosis depending on a variety of intracellular factors, including the activation of caspase-8 and cellular energy status (29).

Obesity and metabolic syndrome are associated with the development of glucose intolerance, hepatic insulin resistance, as well as adipose tissue inflammation, with the eventual progression of NAFLD from steatosis to inflammation and fibrosis. In our study, HFD feeding modeled this progression in both wild-type and RIP3−/− mice. Interestingly, RIP3−/− mice, even on chow diets, exhibited glucose intolerance and increased fasting insulin. The increase in $pSer^{307}$IRS-1 relative to total IRS-1 and expression of genes regulating insulin sensitivity suggests that liver of RIP3−/− mice is insulin resistant, particularly in response to HFD. To date, there is very little data available as to the impact of RIP3 in the maintenance of glucose homeostasis, with only one report indicating the RIP3 can suppress the phosphoinositide-3-kinase/Akt axis in vascular smooth muscle (30). Interestingly, fasting blood glucose and glucose tolerance were not further impacted by HFD in the RIP3−/− mice. Instead, fasting insulin was increased, suggesting that the pancreas was able to release more insulin to maintain fasting glucose. RIP3−/− mice also gained more weight than wild-type mice and exhibited exacerbated adipose tissue inflammation. It is likely that increased weight gain, circulating insulin and inflammation in adipose tissue contributed to the development of greater inflammation and fibrosis in liver in response to HFD feeding. Given the complex interplay between insulin signaling and progression of NAFLD in metabolic syndrome, it will be important in future studies to understand the molecular interactions between RIP3 and insulin signaling.

Regulated cell death pathways are critical to maintaining liver homeostasis and contribute to both disease progression and protection from disease. For example, inhibition of caspase activity or deletion of caspase-8 protects from hepatocyte apoptosis, but can enhance hepatocarcinogenesis (31, 32). Similarly, in the TAK1 knockout model of chronic hepatic inflammation, caspase-8-dependent apoptosis, rather than RIP-3-dependent necroptosis, induces hepatic fibrogenesis and activation of stellate cells (33). Further, RIP3-dependent cell death inhibited carcinogenesis, but contributed to cholestasis in this model (33).

In conclusion, our present findings reveal a protective effect of RIP3 in mice on HFD, in contrast with the deleterious role of RIP3 observed in mice on the MCD diet (16, 17). Our

data indicate that RIP3 protects from the progression of liver inflammation and fibrosis in the context of obesity and impaired glucose homeostasis. Since inhibition of apoptosis with pan-caspase inhibitors has been tested in clinical trials in humans with NASH (34), it is likely that pharmacologic targeting of necroptosis will also be considered. Our findings have great implications in that regard because we have shown clearly that inhibition of necroptosis can lead to increased hepatocyte apoptosis and worsening of liver injury, especially fibrosis. Our data indicate that the intricate balance between the different pathways of programmed cell death in disease progression of NAFLD is likely dependent on the metabolic state of the liver; this interaction should be taken into account when testing new molecular targets.

Supplementary Material

Refer to Web version on PubMed Central for supplementary material.

Acknowledgments

Financial support: This work was supported in part by ABMRF/The Foundation for Alcohol Research (SR); NIH grants R21AA020941 (SR), R37 AA011876 (LEN), P20 AA17069 (LEN); T32DK007319 (RSM); U24DK076174 (CMC) and an ACG Junior Faculty Development Award (NA). The work was also supported in part by the Case Western Reserve University/Cleveland Clinic CTSA UL1RR024989.

Abbreviations

NAFLD	non-alcoholic fatty liver disease
HFD	High fat diet
RIP3	Receptor interacting protein 3
MCP-1	monocyte chemoattractant protein-1
HSC	hepatic stellate cells
NASH	Non-alcoholic steatohepatitis
MLKL	mixed lineage kinase domain-like
TLR	toll-like receptor
DAI	DNA-dependent activator of interferon
MCD	methyl-choline deficient
HOMA-IR	homeostatic model assessment-insulin resistance
αSMA	α-smooth muscle actin
MMP	matrix metalloprotease
RHIM	RIP homotypic interaction motif
TAK1	TGF-β activated-kinase 1

References

1. Ravichandran KS. Beginnings of a good apoptotic meal: the find-me and eat-me signaling pathways. Immunity. 2011; 35:445–455. [PubMed: 22035837]
2. Luedde T, Kaplowitz N, Schwabe RF. Cell death and cell death responses in liver disease: mechanisms and clinical relevance. Gastroenterology. 2014; 147:765–783. e764. [PubMed: 25046161]
3. Guicciardi ME, Gores GJ. Apoptosis: a mechanism of acute and chronic liver injury. Gut. 2005; 54:1024–1033. [PubMed: 15951554]
4. Vick B, Weber A, Urbanik T, Maass T, Teufel A, Krammer PH, Opferman JT, et al. Knockout of myeloid cell leukemia-1 induces liver damage and increases apoptosis susceptibility of murine hepatocytes. Hepatology. 2009; 49:627–636. [PubMed: 19127517]
5. Weber A, Boger R, Vick B, Urbanik T, Haybaeck J, Zoller S, Teufel A, et al. Hepatocyte-specific deletion of the antiapoptotic protein myeloid cell leukemia-1 triggers proliferation and hepatocarcinogenesis in mice. Hepatology. 2010; 51:1226–1236. [PubMed: 20099303]
6. Alkhouri N, Carter-Kent C, Feldstein AE. Apoptosis in nonalcoholic fatty liver disease: diagnostic and therapeutic implications. Expert Rev Gastroenterol Hepatol. 2011; 5:201–212. [PubMed: 21476915]
7. Anstee QM, Concas D, Kudo H, Levene A, Pollard J, Charlton P, Thomas HC, et al. Impact of pan-caspase inhibition in animal models of established steatosis and non-alcoholic steatohepatitis. J Hepatol. 2010; 53:542–550. [PubMed: 20557969]
8. Wu W, Liu P, Li J. Necroptosis: an emerging form of programmed cell death. Crit Rev Oncol Hematol. 2012; 82:249–258. [PubMed: 21962882]
9. Zhang DW, Shao J, Lin J, Zhang N, Lu BJ, Lin SC, Dong MQ, et al. RIP3, an energy metabolism regulator that switches TNF-induced cell death from apoptosis to necrosis. Science. 2009; 325:332–336. [PubMed: 19498109]
10. Han J, Zhong CQ, Zhang DW. Programmed necrosis: backup to and competitor with apoptosis in the immune system. Nat Immunol. 2011; 12:1143–1149. [PubMed: 22089220]
11. Zhou W, Yuan J. Necroptosis in health and diseases. Semin Cell Dev Biol. 2014; 35:14–23. [PubMed: 25087983]
12. Linkermann A, Green DR. Necroptosis. N Engl J Med. 2014; 370:455–465. [PubMed: 24476434]
13. Khan N, Lawlor KE, Murphy JM, Vince JE. More to life than death: molecular determinants of necroptotic and non-necroptotic RIP3 kinase signaling. Curr Opin Immunol. 2014; 26:76–89. [PubMed: 24556404]
14. Ramachandran A, McGill MR, Xie Y, Ni HM, Ding WX, Jaeschke H. Receptor interacting protein kinase 3 is a critical early mediator of acetaminophen-induced hepatocyte necrosis in mice. Hepatology. 2013; 58:2099–2108. [PubMed: 23744808]
15. Roychowdhury S, McMullen MR, Pisano SG, Liu X, Nagy LE. Absence of receptor interacting protein kinase 3 prevents ethanol-induced liver injury. Hepatology. 2013; 57:1773–1783. [PubMed: 23319235]
16. Afonso MB, Rodrigues PM, Carvalho T, Caridade M, Borralho P, Cortez-Pinto H, Castro RE, et al. Necroptosis is a key pathogenic event in human and experimental murine models of non-alcoholic steatohepatitis. Clin Sci (Lond). 2015; 129:721–739. [PubMed: 26201023]
17. Gautheron J, Vucur M, Reisinger F, Cardenas DV, Roderburg C, Koppe C, Kreggenwinkel K, et al. A positive feedback loop between RIP3 and JNK controls non-alcoholic steatohepatitis. EMBO Mol Med. 2014; 6:1062–1074. [PubMed: 24963148]
18. Kohli R, Feldstein AE. NASH animal models: are we there yet? J Hepatol. 2011; 55:941–943. [PubMed: 21708199]
19. Newton K, Sun X, Dixit VM. Kinase RIP3 is dispensable for normal NF-kappa Bs, signaling by the B-cell and T-cell receptors, tumor necrosis factor receptor 1, and Toll-like receptors 2 and 4. Mol Cell Biol. 2004; 24:1464–1469. [PubMed: 14749364]
20. Cohen JI, Roychowdhury S, McMullen MR, Stavitsky AB, Nagy LE. Complement and alcoholic liver disease: role of C1q in the pathogenesis of ethanol-induced liver injury in mice. Gastroenterology. 139:664–674. 674 e661.

21. Roychowdhury S, Chiang DJ, Mandal P, McMullen MR, Liu X, Cohen JI, Pollard J, et al. Inhibition of Apoptosis Protects Mice from Ethanol-Mediated Acceleration of Early Markers of CCl(4) -Induced Fibrosis but not Steatosis or Inflammation. Alcohol Clin Exp Res.
22. Gautheron J, Vucur M, Luedde T. Necroptosis in NASH. Cellular and Molecular Gastroenterology and Hepatology. 2015; 1:264–265.
23. Han W, Xie J, Li L, Liu Z, Hu X. Necrostatin-1 reverts shikonin-induced necroptosis to apoptosis. Apoptosis. 2009; 14:674–686. [PubMed: 19288276]
24. Pasparakis M, Vandenabeele P. Necroptosis and its role in inflammation. Nature. 2015; 517:311–320. [PubMed: 25592536]
25. Mandal P, Berger SB, Pillay S, Moriwaki K, Huang C, Guo H, Lich JD, et al. RIP3 induces apoptosis independent of pronecrotic kinase activity. Mol Cell. 2014; 56:481–495. [PubMed: 25459880]
26. Feldstein AE, Alkhouri N, De Vito R, Alisi A, Lopez R, Nobili V. Serum cytokeratin-18 fragment levels are useful biomarkers for nonalcoholic steatohepatitis in children. Am J Gastroenterol. 2013; 108:1526–1531. [PubMed: 23752877]
27. Witek RP, Stone WC, Karaca FG, Syn WK, Pereira TA, Agboola KM, Omenetti A, et al. Pan-caspase inhibitor VX-166 reduces fibrosis in an animal model of nonalcoholic steatohepatitis. Hepatology. 2009; 50:1421–1430. [PubMed: 19676126]
28. Galluzzi L, Vanden Berghe T, Vanlangenakker N, Buettner S, Eisenberg T, Vandenabeele P, Madeo F, et al. Programmed necrosis from molecules to health and disease. Int Rev Cell Mol Biol. 2011; 289:1–35. [PubMed: 21749897]
29. Christofferson DE, Yuan J. Necroptosis as an alternative form of programmed cell death. Curr Opin Cell Biol. 2010; 22:263–268. [PubMed: 20045303]
30. Li Q, Li G, Lan X, Zheng M, Chen KH, Cao CM, Xiao RP. Receptor interacting protein 3 suppresses vascular smooth muscle cell growth by inhibition of the phosphoinositide 3-kinase-Akt axis. J Biol Chem. 2010; 285:9535–9544. [PubMed: 20042608]
31. Hirsova P, Gores GJ. Death Receptor-Mediated Cell Death and Proinflammatory Signaling in Nonalcoholic Steatohepatitis. Cell Mol Gastroenterol Hepatol. 2015; 1:17–27. [PubMed: 25729762]
32. Liedtke C, Bangen JM, Freimuth J, Beraza N, Lambertz D, Cubero FJ, Hatting M, et al. Loss of caspase-8 protects mice against inflammation-related hepatocarcinogenesis but induces non-apoptotic liver injury. Gastroenterology. 2011; 141:2176–2187. [PubMed: 21878202]
33. Vucur M, Reisinger F, Gautheron J, Janssen J, Roderburg C, Cardenas DV, Kreggenwinkel K, et al. RIP3 inhibits inflammatory hepatocarcinogenesis but promotes cholestasis by controlling caspase-8- and JNK-dependent compensatory cell proliferation. Cell Rep. 2013; 4:776–790. [PubMed: 23972991]
34. Ratziu V, Sheikh MY, Sanyal AJ, Lim JK, Conjeevaram H, Chalasani N, Abdelmalek M, et al. A phase 2, randomized, double-blind, placebo-controlled study of GS-9450 in subjects with nonalcoholic steatohepatitis. Hepatology. 2012; 55:419–428. [PubMed: 22006541]

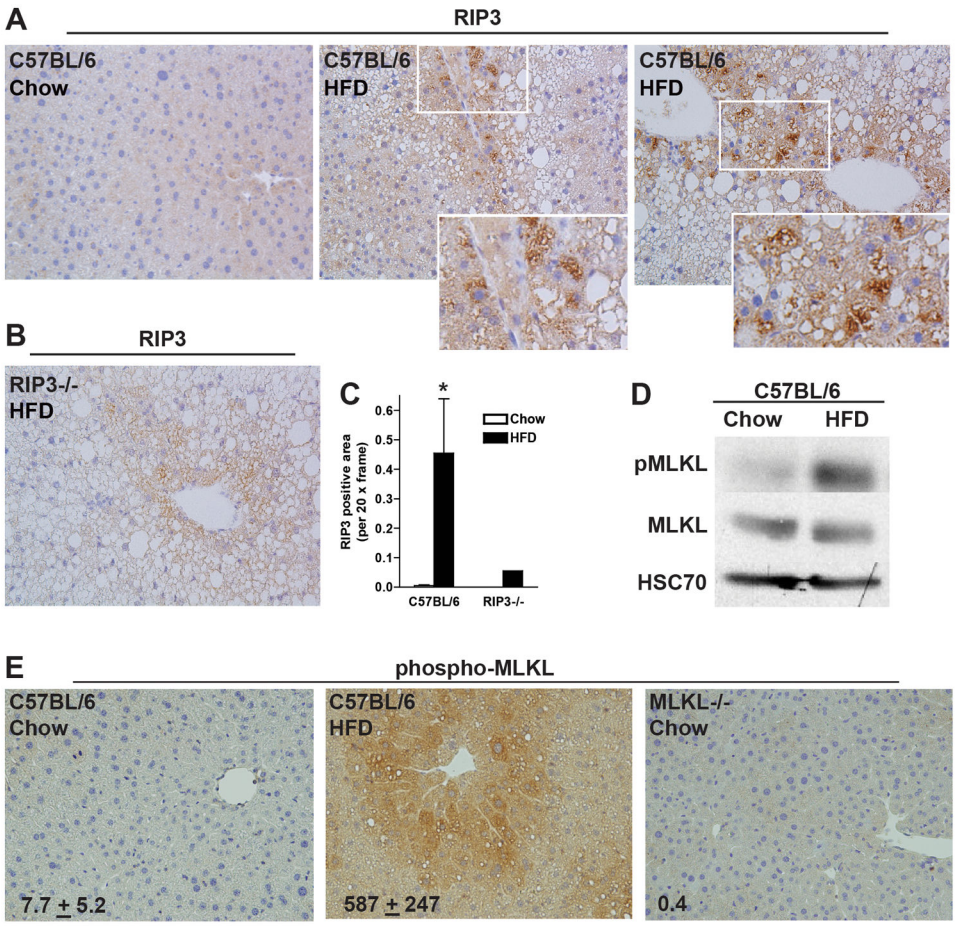

Figure 1. RIP3 expression and phosphorylation of MLKL were increased in mouse liver following high-fat diet feeding

Male C57BL/6 mice were fed HFD or chow for 12 weeks. **(A/B/C)** Paraffin-embedded livers were de-paraffinized followed by immuno-detection for RIP3 in **(A)** C57BL/6 mice after chow or HFD. **(B)** Immuno-detection of RIP3 was carried out in HFD-fed RIP3−/− mice as a negative control. Nuclei were counterstained with hematoxylin. All images were acquired using a 20X objective and analyzed. **(C)** RIP3 positive area was semi-quantified. *$p<0.05$ compared to chow-fed mice. **(D)** Liver lysates were prepared and proteins separated by SDS-electrophoresis. Immunoreactive pMLKL, total MLKL and HSC70, a loading control, were assessed by Western blot. **(E)** Paraffin-embedded livers from C57BL/6 mice were de-paraffinized followed by immuno-detection of phospho-MLKL. Liver sections from MLKL −/− mice were included as a negative control. Images were acquired using a 20X and analyzed.

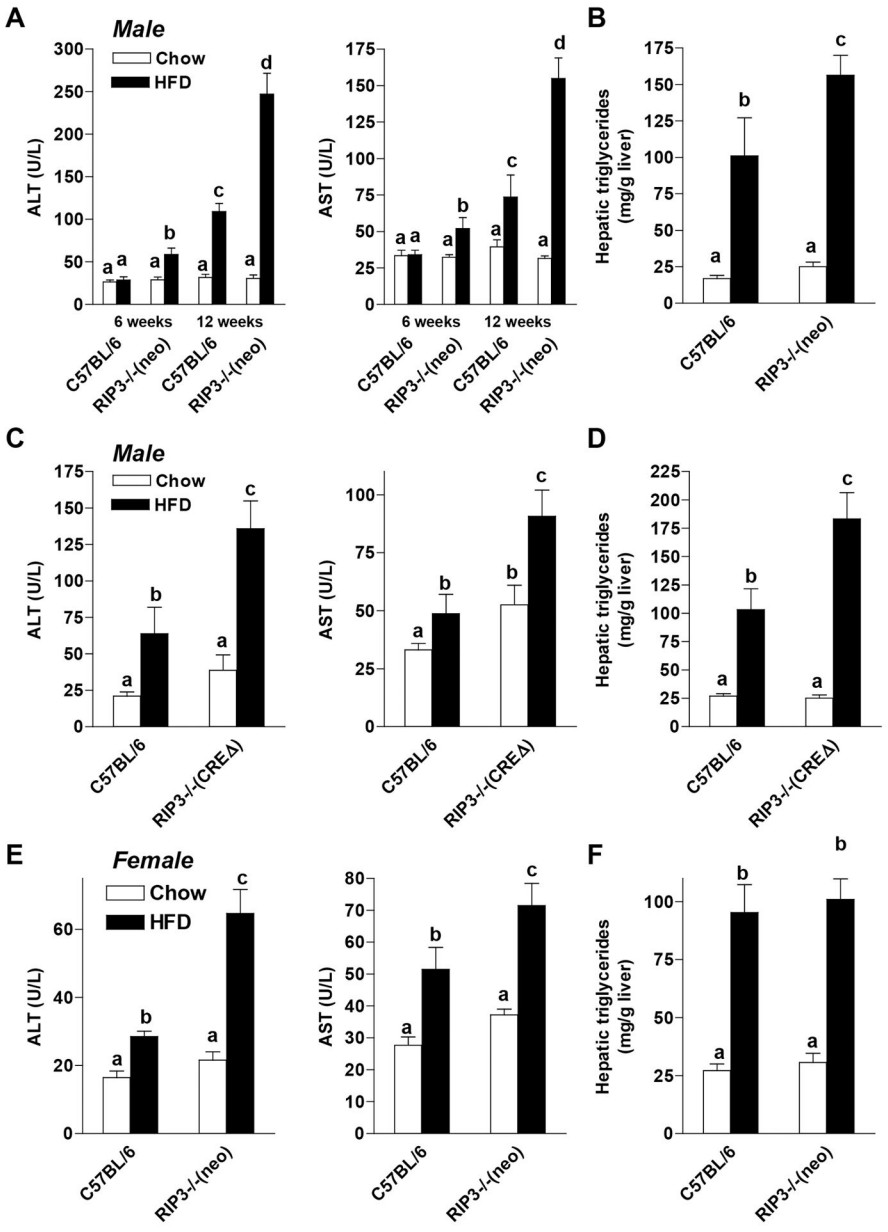

Figure 2. High fat diet-induced liver injury and steatosis were exacerbated in RIP3-deficient mice

(A/B) Male C57BL/6 and RIP3-deficient mice (Strain containing the neomycin cassette (RIP3−/− (neo)); **(C/D)** Male C57BL/6 and RIP3-deficient mice (with the neomycin cassette deleted (RIP3−/− CREΔ)) and (**E/F)** Female C57BL/6 and RIP3-deficient mice (RIP3−/− neo) were fed HFD or chow for up to 6 or 12 weeks. **(A/C/E)** ALT and AST activities were measured in plasma. (**B/D/F)** Hepatic triglyceride content was measured in whole liver homogenate.

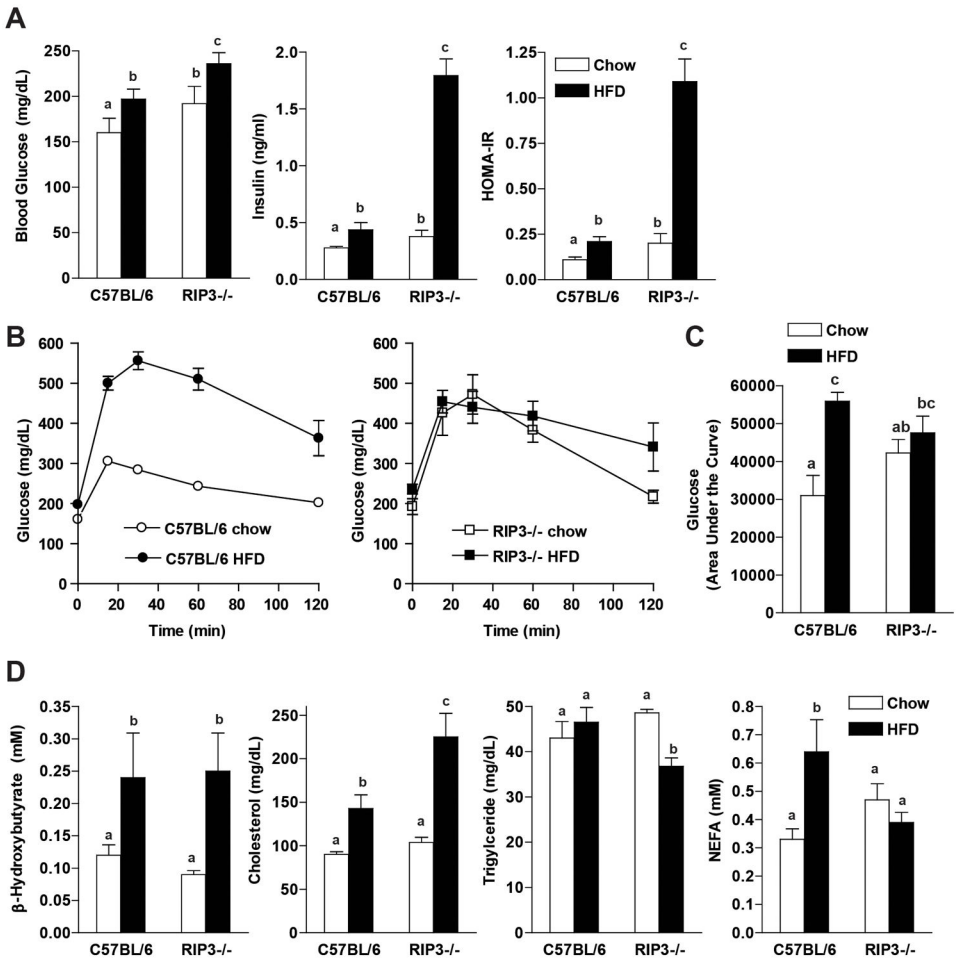

Figure 3. Comparison of metabolic parameters between C57BL/6 and RIP3-deficient mice on chow and high-fat diets

Male C57BL/6 and RIP3-deficient mice (RIP3−/− neo) were fed HFD or chow for 12 weeks. Mice were fasted for 6 hours prior to blood collection and euthanasia. **(A)** Fasting blood glucose was measured from a tail nick using a standard glucometer. Fasting insulin was measured in plasma by ELISA and then HOMA-IR was calculated using the following formula: (fasting glucose (mg/dl) × fasting insulin (ng/ml))/405). **(B)** For glucose tolerance tests, mice were fed HFD or chow for 14 weeks and then received 25% D-glucose solution (2 mg/kg of bodyweight) by intraperitoneal injection. Blood glucose was measured at baseline, 15, 30, 60 and 120 minutes. **(C)** Area under the curves was calculated for statistical analysis. **(D)** Metabolic parameters of lipid metabolism were measured in plasma.

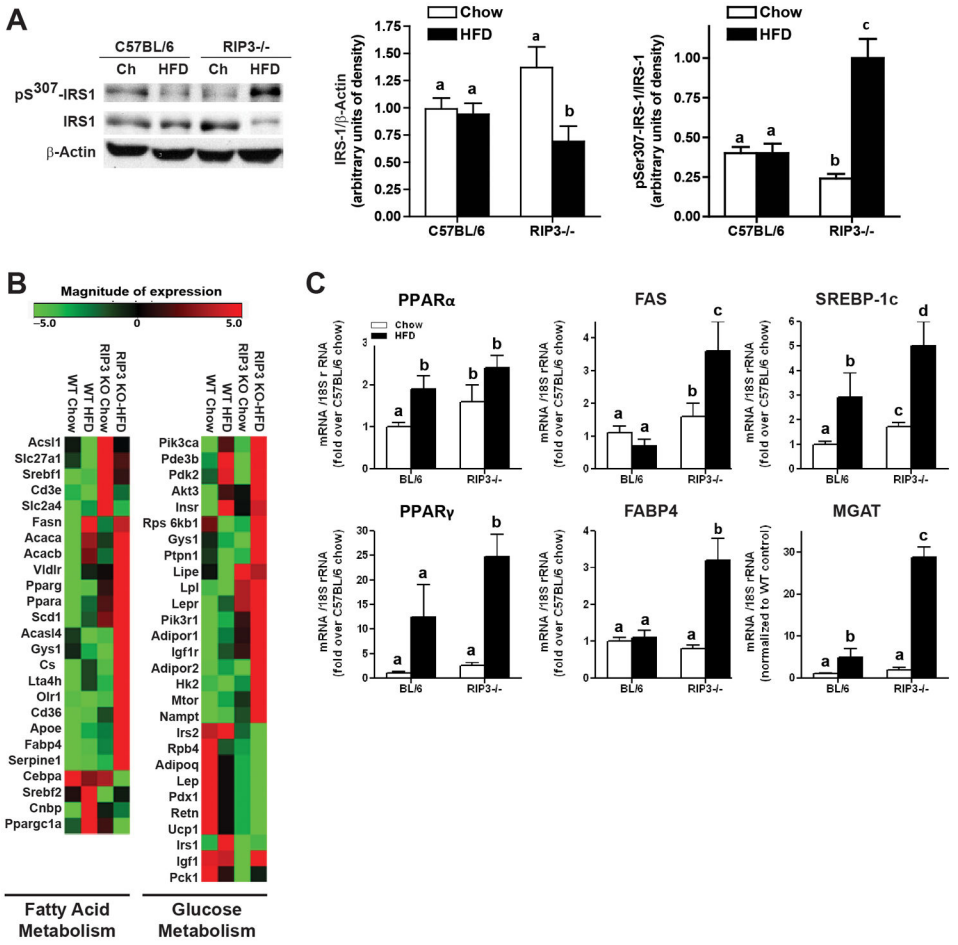

Figure 4. Indicators of insulin signaling and glucose and fatty acid metabolism in RIP3-deficient mice compared to wild-type mice

(A) Male C57BL/6 and RIP3-deficient mice (RIP3−/− neo and RIP3−/− CREΔ) were fed HFD or chow for 12 weeks. Western blot analysis of phosphoSer^{307}-IRS-1 and total IRS-1 was performed in liver lysates and β-actin used as a loading control. **(B)** A pathway array analysis for genes involved in glucose and lipid metabolism was carried out on RNA samples collected from livers of C57BL/6 and RIP3−/− mice fed HFD or chow diets for 12 weeks. **(C)** qRT-PCR validation of changes in the expression of genes identified in the array analysis.

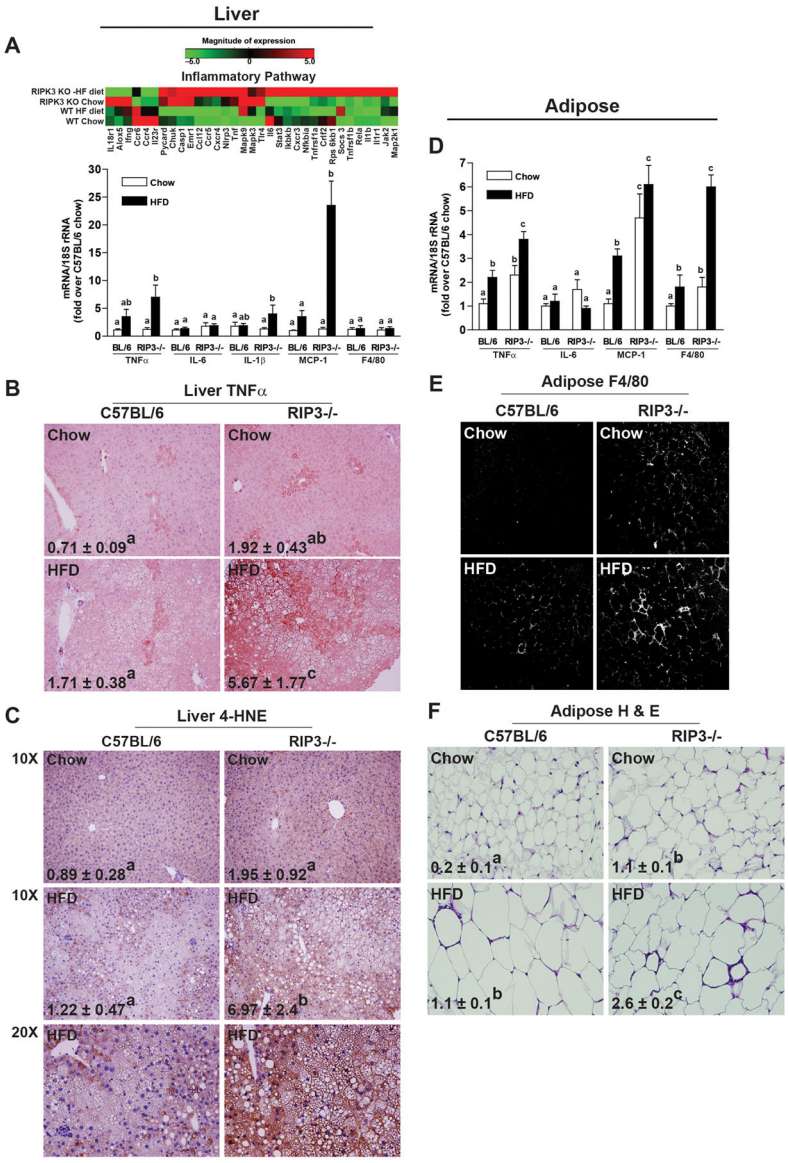

Figure 5. RIP3-deficient mice were more susceptible to high-fat diet-induced inflammatory responses in liver and adipose

Male C57BL/6 and RIP3-deficient mice (RIP3−/− neo) were fed HFD or chow for 12 weeks. **A)** An inflammatory pathway array analysis was carried out. Expression of cytokine, chemokine and F4/80 mRNA was also detected in mouse livers using qRT-PCR measurement. **B)** Paraffin-embedded liver sections were de-paraffinized and stained for TNFα. Images were acquired using a 20X objective and analyzed. **C)** Paraffin embedded sections of liver were deparaffinized and 4-hydroxynonenal adducts were detected by immuno-histochemistry. Images were taken at 10 or 20X, as indicated, and 10X images were analyzed. 20X images are provided to show greater histological detail. **D)** Expression of cytokine, chemokine and F4/80 mRNA was detected in epididymal adipose tissue using qRT-PCR measurement. **E)** Immunoreactive F4/80 protein was evaluated by immunohistochemistry in frozen adipose tissue. **F)** Hematoxylin and eosin stained adipose

tissue illustrates the presence of crown structures after HFD feeding. **(E/F)** Images were acquired using a 40X objective.

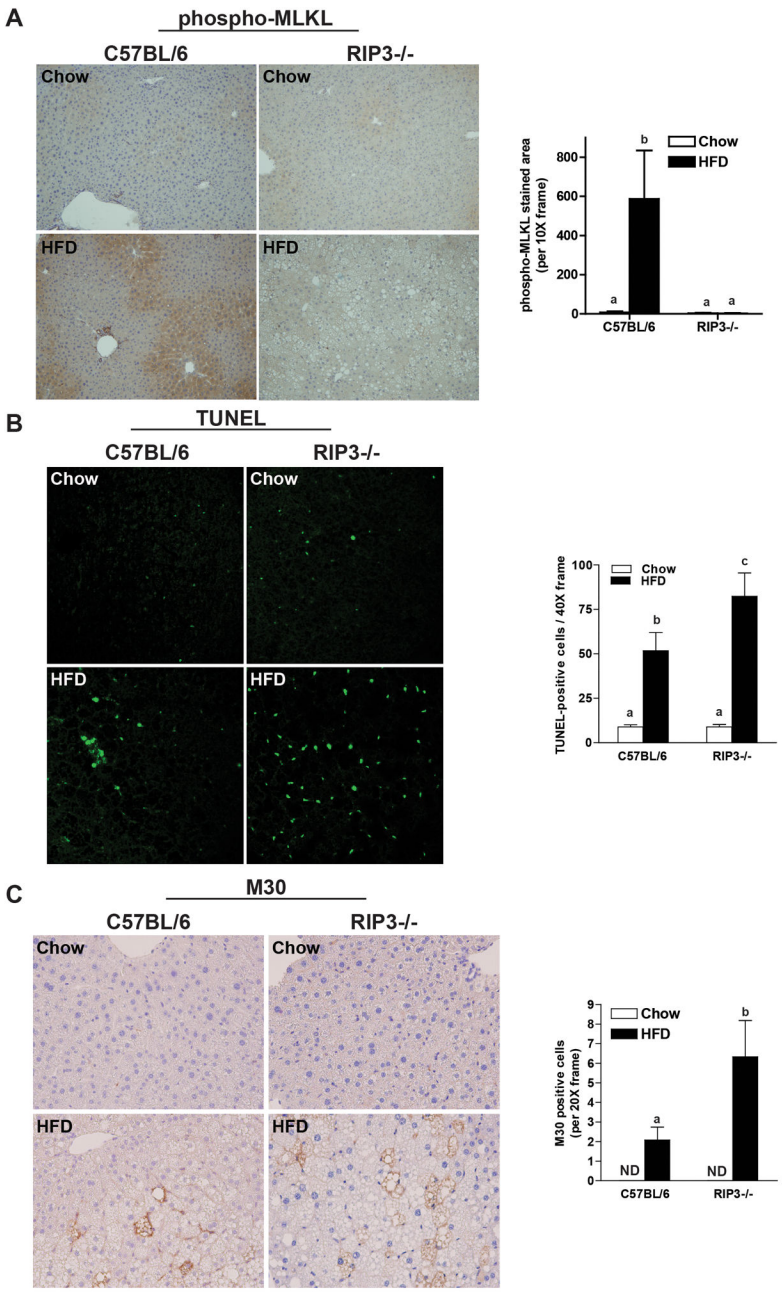

Figure 6. RIP3-deficiency decreases phosphorylation of MLKL, but promotes apoptosis in the liver in response to high-fat diet feeding

Male C57BL/6 and RIP3-deficient mice (RIP3−/− neo) were fed HFD or chow for 12 weeks. Paraffin-embedded livers were de-paraffinized followed by **(A)** phospho-MLKL, **(B)** TUNEL or **(C)** M30 staining. Images were acquired using **(A)** a 10X objective for phospho-MLKL; **(B)** a 40X objective and TUNEL-positive cells were counted and expressed as percent positive of total number of cells per 40X frame and **(C)** a 20X objective and M30-positive cells were counted and expressed as total number of cells per 20X frame. **ND:** M30-positive cells were not detectable in livers of chow-fed mice. *p< 0.05 indicates a difference between genotypes in the HFD groups.

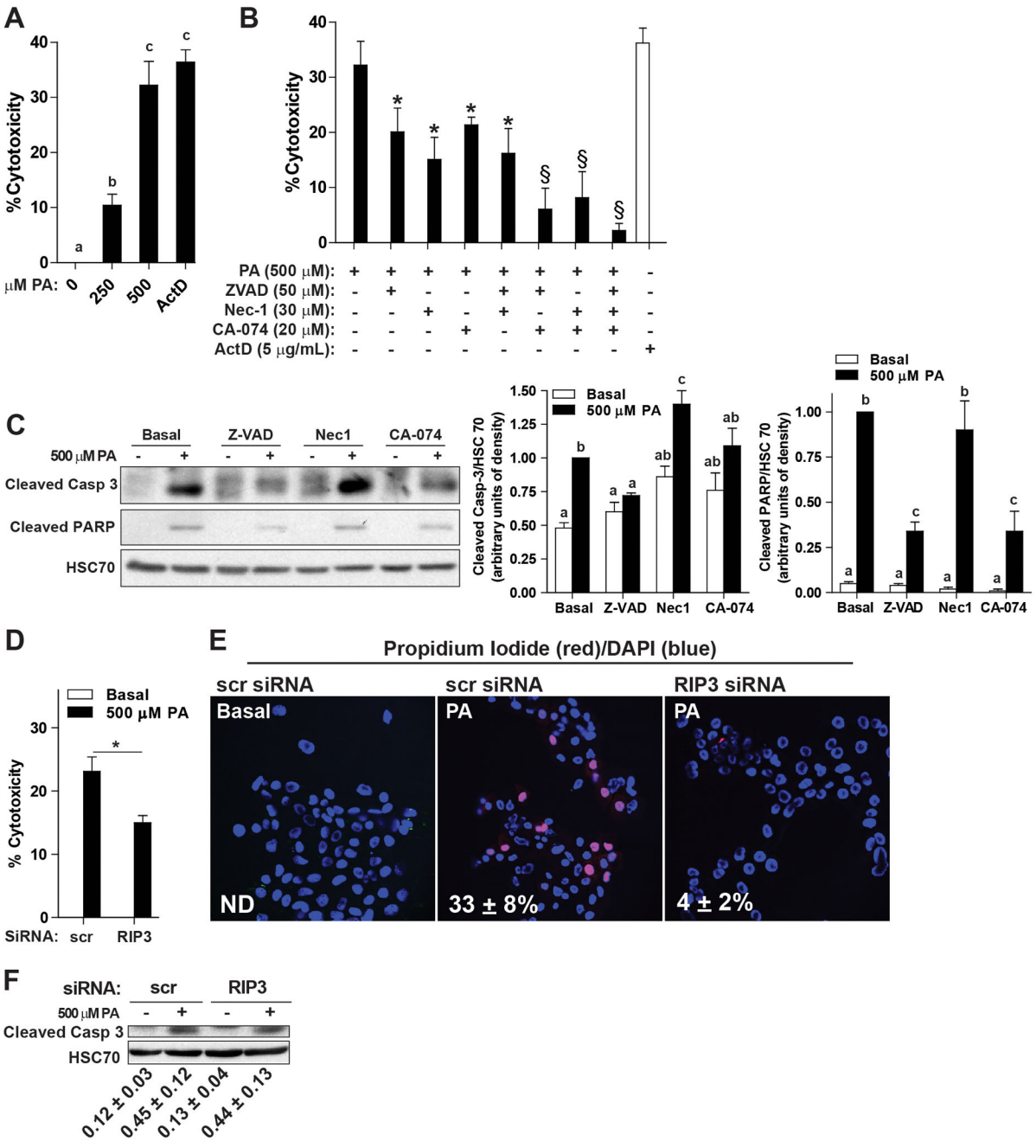

Figure 7. Palmitic acid-induced lipotoxicity occurs via multiple cell death pathways in hepatocytes

AML12 hepatocytes were pre-treated with or without 50 μM Z-VAD, 30 μM necrostatin-1 or 20 μM CA-074 for 2 h and then challenged with or without palmitic acid for 14 h. **(A)** Culture with palmitic acid dose-dependently increased cytotoxicity, assessed by MTS assays. Actinomycin D-treated cells were used as a positive control. **(B)** Pre-treatment with Z-VAD, necrostatin-1 or CA-074 decreased palmitic acid-induced cytotoxicity. *$p<0.05$ compared to palmitic acid alone; §$p<0.05$ compared to cells treated with a single inhibitor. n=4 independent experiments. **(C)** Western blot analysis of the cleavage products of

caspase-3 and PARP were measured in lysates of AML12 cells pre-treated with or without Z-VAD, necrostatin-1 or CA-074 and then challenged with 500μM palmitic acid for 22 h. HSC70 was used as a loading control. **(D/E/F)** AML12 hepatocytes were transfected with scrambled siRNA or siRNA targeted to knock-down RIP3. 24h after transfection, cells were challenged with or without 500 μM palmitic acid. **(D)** Cytotoxicity was assessed by MTS assay. Actinomycin D was used as a positive control for cytotoxicity. **(E)** Propidium iodide (red) staining was evaluated by live cell imaging. PI positive cells were counted in 5 images and expressed relative to the total DAPI (blue) positive cells. **(F)** Western blot analysis of cleaved caspase-3 was measured in lysates. **(D/E/F)** *$p<0.05$, n=4.

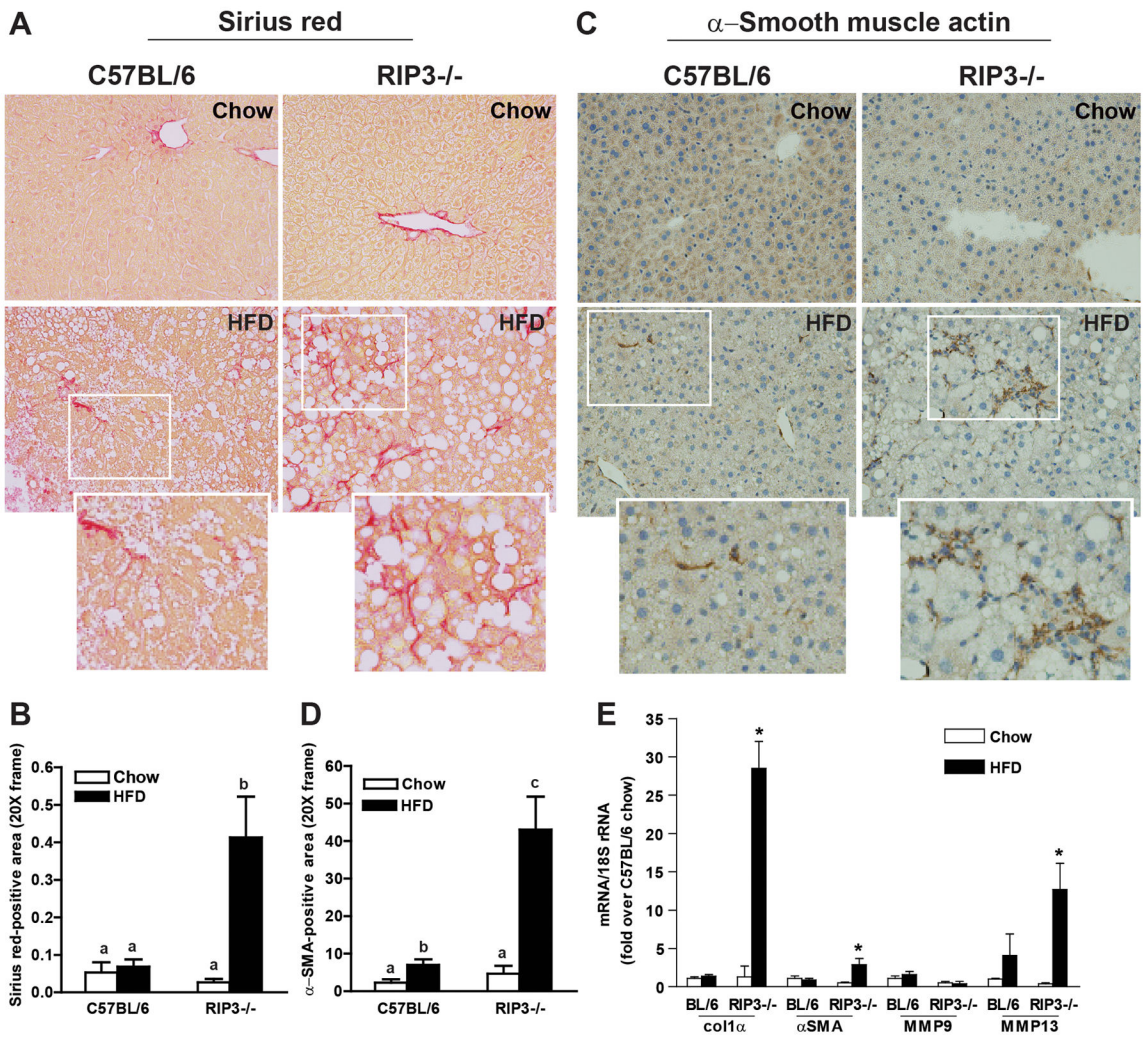

Figure 8. Enhanced markers of fibrosis in RIP3-deficient mice compared to C57BL/6 after high fat diet feeding

Male C57BL/6 and RIP3-deficient mice (RIP3−/− neo) were fed HFD or chow for 12 weeks. Paraffin-embedded liver sections were de-paraffinized and stained for **(A/B)** Sirius red or **(C/D)** αSMA. Images were acquired using 20X objective. **(E)** Expression of mRNA of Col1α, αSMA, MMP9 and MMP13 was measured in liver using qRT-PCR measurement.